Nanophotonics 1 (2012): 221–233 © 2012 Science Wise Publishing & De Gruyter • Berlin • Boston. DOI 10.1515/nanoph-2012-0016

Review

Enhanced nonlinearities using plasmonic nanoantennas

Pai-Yen Chen, Christos Argyropoulos and Andrea Alù*

Department of Electrical and Computer Engineering, University of Texas at Austin, Austin, TX 78712, USA, e-mail: alu@mail.utexas.edu

*Corresponding author

Edited by Niek van Hulst, ICFO, Castadeffels, Spain

Abstract

In this paper, we review and discuss how nanoantennas may be used to largely enhance the nonlinear response of optical materials. For single nanoantennas, there have been tremendous advancements in understanding how to exploit the local field enhancement to boost the nonlinear susceptibility at the surface or sharp edges of plasmonic metals. After an overview of the work in this area, we discuss the possibility of controlling the optical nonlinear response using nanocircuit concepts and of significantly enhancing various nonlinear optical processes using planar arrays of plasmonic nanoantennas loaded with $\chi^{(2)}$ or $\chi^{(3)}$ nonlinear optical materials, forming ultrathin, nanometer-scale nonlinear metasurfaces, as optical nanodevices. We describe how this concept may be used to boost the efficiency of nonlinear wave mixing and optical bistability, due to the large local field enhancement at the nonlinear nanoloads associated with the plasmonic features of suitably tailored nanoantenna designs. We finally discuss three exciting applications of the proposed nonlinear metasurface: dramatically-enhanced frequency conversion efficiency, efficient phase-conjugation for super-resolution imaging and large optical bistabilities.

Keywords: plasmonics; nanoantennas; metamaterials; nonlinear optics.

1. Introduction

In recent years, considerable attention has been paid to the exotic optical response of noble metal nanoparticles [1–4], nanoapertures in metallic films [5] and optical metamaterials [6, 7], which may provide strong *light-matter interaction* at the nanometer scale, supported by localized surface plasmon polaritons (SPP) and associated localized resonances. Random and periodic metallic clusters [8–11] displaying large local field enhancements have shown huge potential to enhance weak optical responses and optical nonlinearities, such as second-harmonic generation (SHG) [11], sum/difference frequency generation [12–14] and surface-enhanced Raman scattering (SERS) [15]. In the realm of linear optics, there have been extensive studies on how plasmons may be focused and confined at a subwavelength scale, giving rise to various optical phenomena and devices based on subdiffractive field enhancement, such as plasmonic waveguides and cavities [2], optical nanoantennas [16–20], superlenses [21–23], cloaking [24, 25] and optical nanocircuitry [26]. Recently, plasmonic nanostructures composed of single [7] or multiple nanoparticles [27] combined with nonlinear elements have also raised significant interest. It has been theoretically and experimentally demonstrated [12, 13] that a pair of noble-metal nanoparticles separated by a gap of few nanometers can largely enhance degenerate wave mixing by several orders of magnitude and provide a highly confined, coherent and frequency-tunable localized photon source [12, 13, 28]. This effect is attributed to the strongly localized electric field at the nano-junction of a nanoparticle dimer and the correspondingly boosted third-order optical nonlinearity supported at the noble-metal surface. Following works [29–33] have demonstrated that optical nonlinearities can be dramatically enhanced by plasmonic resonances of specific nanostructures, as their linear response sensitively depends upon geometry, local environment and the polarization of the impinging wave. In this regard, lasers with tunable wavelength, high peak-intensities (i.e., larger than 1–10 GW/cm^2), short pulse duration (i.e., 200 fs) and repetition rate (i.e., 76 MHz) are usually required to excite the nonlinear response of nanoparticles [12, 13], which may be dramatically enhanced by the large local fields near the plasmonic resonances.

In a different context, there is large interest in translating radio-frequency (RF) antenna concepts to the optical domain, in which plasmonic nanoparticles may be properly tailored as *nanoantennas* [16–20, 34–37]. This concept may allow using nanoantennas as the bridge between nanoscale signal processing and free-space radiation, and to control to a large degree their anomalous plasmonic features, leading to large, controlled and optimized field enhancement in the nanoantenna proximity, especially confined at the nanogap between two tightly coupled antenna arms. This mechanism may be particularly relevant to boost the weak scattering response of nanoparticles and to enhance nonlinear processes and optical spontaneous emission. It may also be used to interpret, tailor, control and optimize the previously mentioned nonlinear enhancement processes at the nanoscale. Finally, it may have exciting implications towards the design of efficient energy harvesting devices [38, 39].

One of the simplest nanoantenna geometries, borrowed from conventional RF technology, consists of two nanorods separated by a small gap (Figure 1). This geometry may be experimentally realized with standard lithographic processes and it can be easily characterized using optical nanocircuit concepts [18–20, 35, 36]. In their linear operation, optical nanodipoles support large and controllable field enhancement at their gap [16], opening up exciting opportunities to

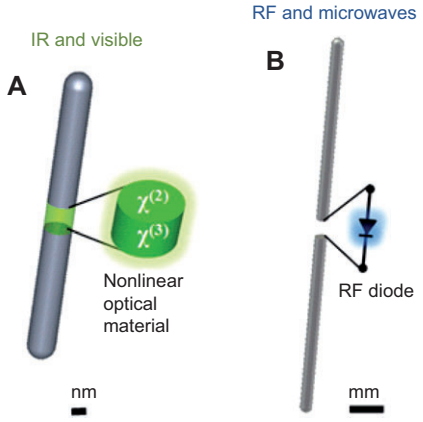

Figure 1 Schematic diagram of: (A) a nanoantenna loaded with nonlinear optical materials at IR or visible frequencies, and (B) a nonlinear antenna loaded with a diode mixer at RF.

extend the nanoantenna concepts to nonlinear optics, with many exciting applications such as high-resolution microscopy and spectroscopy, switching nanodevices and localized light sources [12, 13, 40]. Recently, we have introduced the idea of loading a planar array of optical nanodipole antennas with nonlinear materials (NOM) to achieve significantly enhanced third-order nonlinear effects, which can lead to a variety of optical devices, such as all-optical nanoswitches and nanomemories [33].

Second-order $\chi^{(2)}$ nonlinear effects are usually stronger, but arguably more challenging to induce than third-order $\chi^{(3)}$ nonlinearities, because they usually rely on non-centrosymmetric materials that lack inverse symmetry. In the following, after reviewing the relevant work in the area, we discuss how the large field enhancement in nanodipole antennas may dramatically boost both $\chi^{(2)}$ and $\chi^{(3)}$ effects of nanoparticles embedded in the nanogaps (Figure 1A). Specifically, we provide an overview of applications of planar arrays of nanoantennas loaded with nonlinearities, which may operate analogously to conventional RF nonlinear frequency selective surfaces (FSS) composed of dipole antennas loaded with Schottky or varactor diodes [41] (Figure 1B). This concept can also be extended to bulk optical metamaterials with enhanced nonlinearities, provided that the elementary plasmonic inclusions are properly loaded with NOMs. Self-tuning and wideband nonlinear magnetic metamaterials have been successfully demonstrated at RF and microwaves, loaded with diodes or varactors [42–45].

We also discuss some relevant differences between these two concepts. At low frequencies, nonlinear loads are usually controlled by the *bias voltage* at their terminals, implying that their functionality is practically independent on the size, the filling material of the gap and the distance between the terminals. At optical frequencies, on the contrary, nonlinear nanoloads respond to the local electric field. Therefore, they may experience giant amplification associated with the large local field enhancement at the gap supported by the plasmonic features of the nanoantennas. This property is unique to optical nanoantennas, it cannot be directly translated to lower frequencies and it may provide several exciting advantages for the applications reviewed in the following sections.

Nanoantennas loaded with nonlinearities may provide a flexible design tool to realize efficient nonlinear optical processes at infrared (IR) and visible frequencies through the careful tuning of the geometry or of the loading material, based on the optical nanocircuit concept [26]. Indeed the mutual coupling and interactions among closely spaced nanoantennas, when arranged in planar arrays or *metasurfaces*, may further enhance nonlinearities of natural NOM. As a result, despite the small volume of a NOM load and its naturally weak response, the nanoantenna geometry can significantly enhance and enable nonlinear wave-mixing and other intriguing nonlinear optical properties at the nanoscale, with relatively low optical intensities.

This review paper is organized as follows: in sections 2 and 3, we discuss and review scenarios in which nanoantennas have been used to induce strong nonlinear optical processes at the nanoscale. First, we review some recently observed nonlinear optical responses in nanoantennas and optical metamaterials, due to intrinsic $\chi^{(3)}$ nonlinearities of plasmonic-metals and the strong local field enhancement at the surface and sharp edge of nanoantennas. We then discuss how these concepts may be controlled and optimized applying nanocircuit models. In section 3, we discuss an analytical homogenization model for nonlinear metasurfaces formed as planar arrays of nonlinear nanoantennas, which may be applied to model few configurations of interest, described in detail in section 4: (1) second harmonic generation (SHG) with $\chi^{(2)}$ NOM load, (2) phase conjugation by degenerate four wave mixing (FWM), which can be achieved with $\chi^{(3)}$ NOM load, and (3) optical bistability with $\chi^{(3)}$ NOM load. Finally, a short conclusion on the perspective of using nanoantennas and their array combination for nonlinear operation is presented in section 5.

2. Plasmonic nanoantennas with enhanced nonlinear response

The nonlinear properties of plasmonic materials, in particular gold [29], are well understood. At the plasmon resonance, multiphoton processes may be amplified by the enhanced electric field within or in proximity of metallic nanoparticles. For example, it has been observed that size-dependent third harmonic generation (THG) is feasible in gold nanoparticles [29, 46, 47]. It is interesting to note that THG is induced at the particle surface, with a nonlinear dipole proportional to the area of the sphere rather than to its volume [29], due to the small skin depth of metals and the corresponding small field penetration. Nanoantennas operating at infrared and visible frequencies are largely dependent on the plasmonic properties of metals [34, 48], whose behavior in the linear optical regime is well described by free electrons and additional interband transitions that produce frequency dispersion and support surface-plasmons responsible for the characteristic color of metals [48]. When the size of the nanostructures becomes comparable with the electron mean free path, such as

at corners, tips and gaps, nonlocal and quantum effects come into play [49, 50] and, interestingly, metals exhibit nonnegligible nonlinear response [48, 51]. In previous literature [48, 51], the $\chi^{(3)}$ value of gold has been reported to be 1 nm^2/V^2 However, in general, optical nonlinearities of plasmonic metals are largely unexplored and so far only few noble metal nanostructures have been studied, including SHG [11, 31], THG [29, 30] and FWM [12, 13].

Recently, it has been reported that nonlinear multi-wave mixing can be excited at the nanojunction between plasmonic dimers, as a result of the strong local field intensity, rendering a highly confined, coherent and frequency tunable local photon source [12, 13, 52]. In reference [12], Novotny and his group have demonstrated that, by reducing the separation between a pair of gold nanoparticles, the intensity of the degenerate FWM signal can be enhanced by four orders of magnitude.

Figure 2 demonstrates the experimental setup and measured emission spectrum of this wave-mixing nanodevice, where a high-peak intensity and short-pulse laser with tunable frequency ω_1 pumps an optical parametric oscillator (OPO), which provides pulses of the same duration at a tunable frequency ω_2. Consequently, as observed in Figure 2, one may obtain boosted nonlinear signal $\omega_{FWM}=2\omega_1-\omega_2$, which originates from the third-order nonlinear polarization $\mathbf{P}^{(3)}(2\omega_1-\omega_2)=\chi^{(3)}\mathbf{E}(\omega_1)\mathbf{E}(\omega_1)\mathbf{E}(\omega_2)$, as well as very weak second-order responses at frequencies $2\omega_1$, $2\omega_2$, and $\omega_1+\omega_2$ (due to the unintentional asymmetry in nanoantenna geometry). For this geometry the FWM conversion efficiency is highly polarization dependent, with the signal being strongest, when the excitation field is polarized along the dimer axis. It has been reported that, at very close interparticle distances

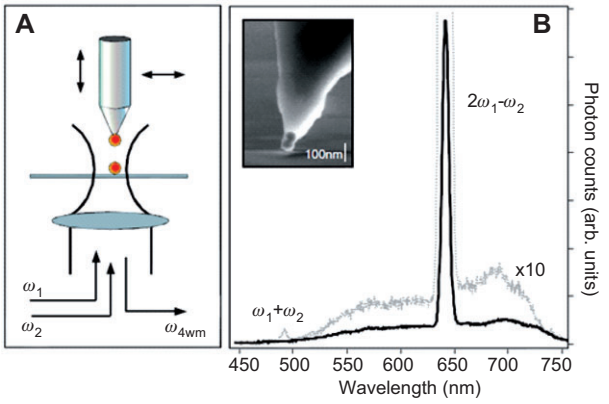

Figure 2 (A) Experimental setup for multi-wave mixing by a single nanoantenna formed by a pair of gold nanoparticles (with a diameter of 60 nm). The laser pulses, at center frequencies ω_1 and ω_2, both locally irradiate the dimer nanoantenna, which is adhered on a glass fiber [see SEM image in the inset of Figure 2B], with its motion being accurately controlled by a PEZ-nanomotor. (B) Emission spectrum of the nanoantenna excited with pulsed lasers of wavelengths $\omega_1=830$ nm and $\omega_2=1185$ nm. The peak nonlinear signal $2\omega_2-\omega_1$ is measured, and the superimposed gray-dotted curve shows the spectrum of two nanoparticles with unequal size (60 nm and 100 nm in diameter). (Source: Ref. [12]).

[13], sensitive fluctuations of the *photon count rate* may be observed, since small changes in the contact region may give rise to huge variations in the spectral response.

When the interparticle distance decreases, the linear plasmon resonance shifts towards longer wavelengths, due to the corresponding increase in load capacitance; a dispersion that can be easily explained using the nanocircuit approach [16–20]. Therefore, by tuning the nanogap distance, the plasmonic resonance of the nanoantenna may be tuned to the FWM frequency $\omega_{FWM}=2\omega_1-\omega_2$, leading to greatly enhanced nonlinear optical response. In this scenario, bursts of narrowband photons can be generated with a tunable center frequency, depending on the gap size and frequencies of excitation ω_1 and ω_2. Once gold nanoparticles touch, or quantum effects arise as the gap dimensions shrink [53] to less than a few nm, the resonance abruptly shifts to much lower frequencies. FWM signals can be further enhanced by coupling to a third nanoparticle placed in close proximity to the dimer, which is somehow analogous to a closed-loop nanocircuit [26]. This concept has been further extended to near-field optical imaging and spectroscopy [13, 52], by using nonlinear responses generated by a pair of gold nanoparticles as a localized photon source for fluorescence and extinction imaging. In this context, photons at frequency $\omega_{FWM}=2\omega_1-\omega_2$ can be highly localized, with large temporal coherence and, more importantly, with frequency tunability. As a result, high-resolution fluorescence imaging can be obtained by tuning ω_{FWM} into the absorption spectrum of fluorescent sample molecules. Since the wavelength of the FWM signal can be adjusted over a wide spectral range by slightly detuning the pumping frequencies ω_1 and ω_2, the plasmonic dimer is ideally suitable for high-resolution fluorescence imaging and local extinction measurements.

It may be also possible to excite second-order nonlinearities by synthesizing asymmetric nanostructures, such as split-ring resonators [32] or T-shaped nanodimers [31], which inherently possess asymmetric field distributions at the particle perimeter. It has been experimentally demonstrated [31] that the asymmetrically distributed local electric fields in noncentrosymmetric gold nanodimers may produce a large SHG response.

In the previously discussed plasmonic nanostructures, the SHG enhancement process was limited to the plasmonic interface, as fields rapidly decay inside metals. Recently, Pu et al. [11] have demonstrated that symmetric and resonant composite plasmonic structures loaded with $\chi^{(2)}$ – NOMs may also exhibit greatly enhanced SHG responses. Figure 3A shows a nonlinear plasmonic core-shell optical nanocavity [11], where a noncentrosymmetric ($BaTiO_3$) medium, which utilizes the entire mode volume for even-order nonlinear optical processes, is incorporated within a plasmonic (gold) nanocavity. Figure 3B shows the normalized emission spectra of $BaTiO_3$-gold core-shell nanocavities (blue solid circles) and pure gold nanoparticles (green solid squares). It is evident that the core-shell nanostructure shows remarkably higher SHG responses, compared to the unloaded plasmonic particle. If we compare the composite plasmonic nanoparticle with a bare 100 nm $BaTiO_3$ nanocrystal, an enhancement of over 500 times in the

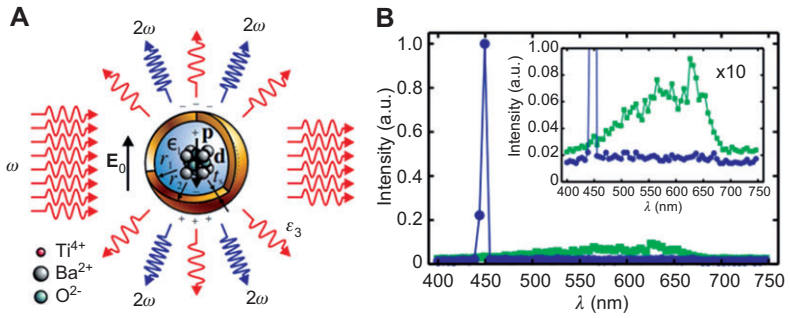

Figure 3 (A) Principle and geometry of plasmonic-enhanced SHG nanocavity. (B) Emission spectra of nominally 100 nm $BaTiO_3$-gold core-shell nanocavities (blue solid circles) and 200 nm gold nanoparticles (green solid squares) normalized to the SHG peak intensity of the core-shell nanostructures. The inset shows the same data magnified by 10 in magnitude, where the two-photon photoluminescence of 200 nm gold nanoparticles is more visible. (Source: Ref. [11]).

SHG radiation power was obtained. This device may enable efficient, subwavelength, coherent nanosources.

Another exciting optical application of asymmetric nanoantenna geometries consists in electromagnetically induced transparency (EIT) [54, 55] or Fano resonances [56], supporting a sharp transmission band within a broader absorption region. Such phenomena show great potential for slow light, novel sensors and low-loss metamaterials [54–56]. It is expected that controllable, strongly localized electric fields within the small-volume of plasmonic nanostructures may pave the way to viable nanoscale optical sensors with high sensitivity. It has been theoretically studied [54] and experimentally verified [55] that a plasmonic nanostructure comprising of asymmetrically stacked nanoantennas can represent the electromagnetic analog of quantum Fano-type interference effects. Reference [54], as an example, reports one possible plasmonic EIT design, for which a dipole nanoantenna with a broad linewidth (bright mode) is coupled to an underlying quadrupole nanoantenna, whose narrow linewidth (dark mode) is limited by non-radiative Drude damping. Due to substantial suppression of nonradiative losses, a very narrow transparency window with high modulation depth was experimentally observed. Being able to engineer and optimize these asymmetric resonant nanostructures may open new exciting possibilities for nonlinear optical applications, including enhanced $\chi^{(2)}$ effects and nonlinear EIT at the nanoscale. Recently, also the combination of third-order nonlinearities with dipole-dipole Fano-type resonances was demonstrated [57], showing great potential towards the design of efficient all-optical switches and nanomemories.

As outlined above, plasmonic-enhanced nonlinearities in nanoantennas and related nanostructures may be achieved by tuning their resonant frequency at the pumping wave frequency or at the frequency of the resulting nonlinear response of interest. Tunable, localized photon sources hold great potential for high-resolution imaging, spectroscopy and sensing, like single quantum dots, molecules, or ions. In particular, nonlinear nanoantennas may serve as promising frequency conversion devices at a single-photon level to realize single-photon transistors [58], where the energy of a single photon is employed to switch between different states. Even if it may be convenient to exploit the relatively strong intrinsic nonlinearity of metals for these nonlinear operations, another possibility consists in loading suitably tailored nonlinear nanoparticles at the gap of dimers and dipole antennas (Figure 1A). This approach may provide even stronger and more penetrable second- or third-order nonlinearities and may make easier the full characterization and modeling of their nonlinear response using the nanocircuit concepts. Dipole antennas loaded with nonlinear circuit elements, such as diodes and varactors (Figure 1B), are commonly used at RF and microwaves. Translating these concepts to optics, nano-dipole antennas loaded with nonlinear optical materials are considered one of the most viable nonlinear nanoantenna geometries, which are suitable for general-purpose nonlinear optical applications. This design (Figure 1A) allows exploiting the large and controllable field enhancement achieved at the nanogap, associated with the nanoantennas' plasmonic features.

In the following sections, we concentrate on this last possibility, reviewing modeling and applications of nonlinearly loaded nanodipole antennas that may be rigorously modeled in array configurations and may realize a flexible design tool to strongly enhance second-order and/or third-order optical nonlinearities. In this approach, nonlinear nanoparticles are specifically loaded at the nanogap of a dimer or dipole, taking advantage of the largely uniform and strong local field enhancement at the plasmon resonance.

3. Modeling of nonlinear metasurfaces

It is well-known that the shortening of guided wavelength for a mode propagating along a plasmonic nanorod with respect to the free-space wavelength [12–20] makes a nanodipole antenna resonate at a much shorter length than a conventional RF dipole of similar electrical length. This implies that it may be possible to realize dense arrays of resonant nanoantennas with periods much smaller than the wavelength of excitation and effectively realize artificial nonlinear metasurfaces, as shown in Figure 4. In their linear operation, the main extinction resonances of the metasurface arise from the collective Rayleigh scattering (with dipolar radiation signature) of the nanoantennas, for which the reflection peak of the

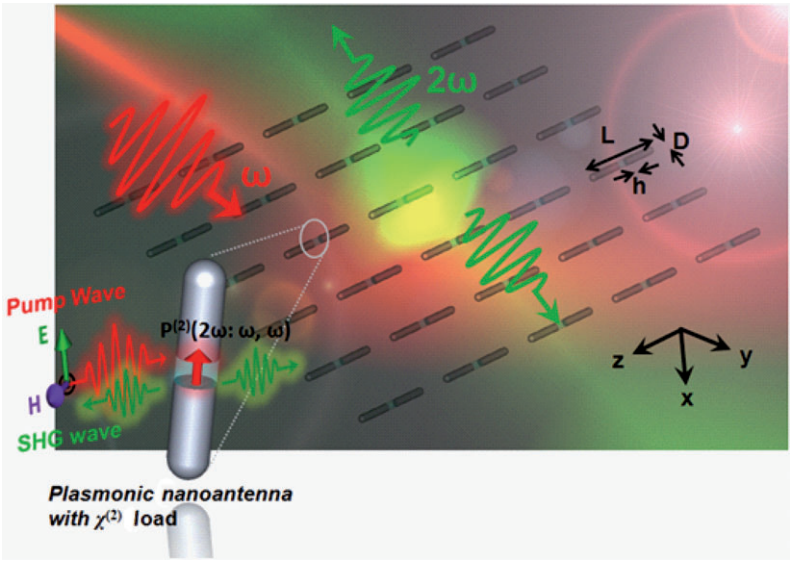

Figure 4 Design and operation principle of a single nonlinear nanoantenna and of a nanoscale SHG frequency conversion system, consisting of a plasmonic metasurface made of an array of silver nanoantennas loaded with $\chi^{(2)}$ nonlinear optical materials, which induces nonlinear frequency mixing at each nanoload.

metasurface depends on the plasmon oscillation length of the nanoantennas. Here, an individual nanoantenna is assembled as a pair of closely spaced silver nanowires with a nanoparticle load in the gap, whose relative permittivity in the linear region is ε_L. The relative permittivity of silver is described by the Drude-dispersion model obtained from experimental data [59] $\varepsilon_{Ag}=\varepsilon_\infty-\omega_p^2/\left[\omega\left(\omega+i\gamma\right)\right]$, with $\omega_p/2\pi=2175$ THz, $\gamma/2\pi=4.35$ THz and $\varepsilon_\infty=5$. The physical dimensions of each nanoantenna are $L=135$ nm, $D=10$ nm and $h=12.5$ nm (see Figure 4). Here, commercially available Maxwell's equation solver, CST Microwave Studio [60], was used to perform the full-wave, time-domain simulations, based on the finite-integration technique. Figures 5A and B show our calculation of the normalized polarizability α (normalized to $6\pi\varepsilon_0/k_0^3$), which relates the induced linear dipole moment to the local electric field at a given frequency, and the field enhancement at the nanogap for an individual nanoantenna for different values of ε_L load. The inset of Figure 5A shows the corresponding far-field radiation pattern, consisting of a typical dipolar radiation, as expected due to the small nanoantenna size. It can be seen, comparing the two panels, that large local field enhancement may be obtained at the nanoantenna resonance inside the gap (Figure 5B) [61]. Using the optical nanocircuit paradigm [16], we can tune and control the resonance frequency to a large degree by properly selecting the equivalent impedance of the nanoload, as shown by the different curves in Figure 5. This is possible because the local confinement of the electric field, as well as its specific polarization at the nanoload, allows quantitatively defining the optical impedance of the nanoantenna and the load, and model the problem as a circuit resonance. To many degrees, this becomes the optical analog of changing the inductive load of a nonlinear

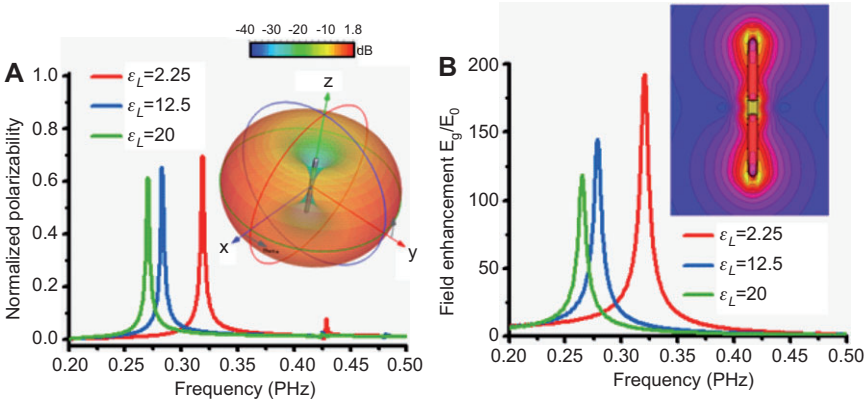

Figure 5 Magnitude of (A) normalized polarizability for a single plasmonic nanoantenna and (B) local field enhancement at the nanogap, for different values of relative permittivity ε_L of the nanoload. The inset of Figure 5A shows the far-field dipolar radiation pattern at resonance. The inset of Figure 5B shows the near-field electric field distribution of an individual nanoantenna in the linear regime, showing strong field intensity in the gap at the plasmonic resonance.

antenna by turning its knob or varying the applied voltage on a varactor [16].

We extend in the following our recently proposed homogenization model of linear metasurfaces [62, 63] to this nonlinear regime. Through the description of the nanoantenna array as a homogenized nonlinear impedance surface, we can greatly simplify its design and optimization for various nonlinear optical applications. For simplicity, we start with second-order nonlinear metasurfaces loaded with $\chi^{(2)}$ NOM nanoparticles. However, the same approach can be used to homogenize third-order nonlinear metasurfaces.

The wave interaction with nanodipole antennas is obviously maximized when the polarization of the exciting electric field is aligned parallel to the dipole-arm axis $\hat{z}$ (Figure 4). We consider an illumination at frequencies ω_1 and ω_2 composed of transverse-electric (TE) plane waves with electric field polarized along the $\hat{z}$-axis, with arbitrary wave vectors. We assume that the nanoantenna length is subwavelength at these frequencies, as they operate near their resonance, such that they may be described in terms of the polarizability α (Figure 4A). The collective scattering at the two frequencies and at the mixing frequency $\omega_1+\omega_2$ is composed of only the dominant diffraction order. This is equivalent to assume that the array may be described in the far-field as a homogenous averaged surface current sheet radiating plane waves at the relevant frequencies on both sides of the metasurface. The inherently subwavelength dimension of each nanoantenna, and the condition that the individual elements of the array are not too close to each other, makes possible to neglect quadrupoles and higher-order multipoles in considering the mutual coupling in the array.

The nonlinear averaged polarization vector at the location of one nanoantenna can be related to the macroscopic local field $\mathbf{E}_{loc}$ at the mixing frequency as

$$\mathbf{p}^{(2)}_{NxNy}(\omega_1+\omega_2;\omega_1,\omega_2)=\alpha\left(\omega_1+\omega_2\right)\mathbf{E}_{loc}(\omega_1+\omega_2) +\beta(\omega_1+\omega_2;\omega_1,\omega_2)\mathbf{E}_{loc}(\omega_1)E_{loc}(\omega_2) \quad (1)$$

where $\alpha(\omega_1+\omega_2)$ is the linear polarizability at the mixing frequency, $\beta(\omega_1+\omega_2;\ \omega_1,\ \omega_2)\simeq\chi^{(2)}\ (\varepsilon_0\pi D^2h/4)f_{rad}(\omega_1+\omega_2)f_g(\omega_1)f_g(\omega_2)$ is the nonlinear hyperpolarizability and f_{rad}, f_g represent the enhancement factors at the relevant frequencies due to nanoantenna radiation and localization properties. These factors may be obtained from linear full-wave simulations, as presented in Figure 5. Rigorously considering the whole dynamic coupling among nanoantennas in the array, we may write (1) as:

$$\begin{aligned}\mathbf{p}^{(2)}_{N_y'N_z'}(\omega_1+\omega_2;\omega_1,\omega_2)&=\alpha\left(\omega_1+\omega_2\right)\mathbf{E}_{loc}(\omega_1+\omega_2)+\beta(\omega_1+\omega_2;\omega_1,\omega_2)\mathbf{E}_{loc}(\omega_1)\mathbf{E}_{loc}(\omega_2)\\ &=\alpha\left(\omega_1+\omega_2\right)\sum_{(N_y,N_z)\neq(N_y',N_z')}\mathbf{G}^{\omega_1+\omega_2}(r_{N_yN_z}-r_{N_y',N_z'})\cdot\frac{\mathbf{p}^{(2)}_{N_y'N_z'}(\omega_1+\omega_2)}{\varepsilon_0}\\ &+\beta(\omega_1+\omega_2;\omega_1,\omega_2)\left[\mathbf{E}_{inc}(\omega_1)+\sum_{(N_y,N_z)\neq(N_y',N_z')}\mathbf{G}^{\omega_1}(\mathbf{r}_{N_yN_z}-\mathbf{r}_{N_y',N_z'})\cdot\frac{\mathbf{p}^{(1)}_{N_y'N_z'}(\omega_1)}{\varepsilon_0}\right]\\ &\cdot\left[\mathbf{E}_{inc}(\omega_2)+\sum_{(N_y,N_z)\neq(N_y',N_z')}\mathbf{G}^{\omega_2}(\mathbf{r}_{N_yN_z}-\mathbf{r}_{N_y',N_z'})\cdot\frac{\mathbf{p}^{(1)}_{N_y'N_z'}(\omega_2)}{\varepsilon_0}\right],\end{aligned} \quad (2)$$

where N_y and N_z are integer numbers associated with the nanoantenna coordinates $y=N_ya_y$ and $z=N_za_z$, with a_y and a_z being the array periods along the two Cartesian axis, $\mathbf{G}(\mathbf{r}_{lmn})$ is the electric dyadic Green's function [62, 63]

$$\mathbf{G}(\mathbf{r}_{N_xN_y})=(\nabla\nabla+k^2\overline{\overline{\mathbf{I}}})\frac{e^{-jk_0r}}{4\pi r}.$$

After some algebraic manipulation, we may write (2) as:

$$\begin{aligned}\mathbf{p}^{(2)}_{00}(\omega_1+\omega_2;\omega_1,\omega_2)&=\hat{z}\,\boldsymbol{p}^{(2)}_{00}(\omega_1+\omega_2)\\ &=\beta(\omega_1+\omega_2:\omega_1,\omega_2)\Im(\omega_1+\omega_2)\\ &\ \Im(\omega_1)\Im(\omega_2)\mathbf{E}_{inc}(\omega_1)\mathbf{E}_{inc}(\omega_2),\end{aligned} \quad (3)$$

where $\Im$ is the local field correction factor:

$$\Im(\omega_i)=\left[1-\varepsilon_0^{-1}\alpha\left(\omega_i\right)C^{\omega_i}\right]^{-1} \quad (4)$$

and C is the interaction constant, which takes into account the dynamic coupling within the array and can be calculated as a fast-converging series using Poisson summations [64]:

$$C^{\omega_i}=\sum_{(N_y,N_z)\neq(0,0)}\mathbf{G}^{\omega_i}(\mathbf{r}_{N_yN_z})\cdot\hat{z}\cdot\hat{z} \quad (5)$$

The averaged surface current on the metasurface, induced by the collective response of the induced nonlinear dipole moments $\mathbf{p}^{(2)}$ is then given by

$$\begin{aligned}\mathbf{J}^{NL}_{av}&=\hat{z}J^{NL}_{av}=\frac{-i\left(\omega_1+\omega_2\right)\mathbf{p}^{(2)}_{00}\left(\omega_1+\omega_2;\omega_1,\omega_2\right)}{d_yd_z}\\ &=\hat{z}\frac{-i\left(\omega_1+\omega_2\right)}{d_yd_z}\beta(\omega_1+\omega_2:\omega_1,\omega_2)\Im(\omega_1+\omega_2)\\ &\ \Im(\omega_1)\Im(\omega_2)E_{p1}E_{p2}\end{aligned} \quad (6)$$

For ultrathin metasurfaces with subwavelength periodicity, the radiated plane waves at the mixing frequency $\omega_1+\omega_2$ will be emitted on both sides of the metasurface with equal complex amplitudes, as a function of the amplitudes of the pumping waves E_{p1} and E_{p2} at frequencies ω_1 and ω_2, respectively.

4. Applications of nonlinear metasurfaces

In this section, we discuss and review three potential applications of nonlinear plasmonic metasurfaces formed by

nanodipole antennas, which may be described using the analytical model discussed in the previous section. The goal is to review these applications in order to highlight the powerful tools offered by the nanocircuit model of nonlinearly loaded nanoantennas in various practical scenarios of interest and present novel numerical results and physical insights on their functionality.

4.1. Second harmonic generation and frequency doubling

Second harmonic generation (SHG) is the nonlinear process of converting a portion of the impinging energy at the fundamental frequency ω into the double frequency 2ω. It may be obtained as a degenerate three-wave mixing ($2\omega=\omega+\omega$) process based on $\chi^{(2)}$ nonlinearity. In this section, we will discuss enhanced SHG over a single planar metasurface using the nanoantenna arrays discussed in the previous section with $\chi^{(2)}$ nanoloads (Figure 4). We will show that, despite the small volume of $\chi^{(2)}$ NOM nanoloads, a *metasurface nanomixer* or *frequency doubler* may be realized at optical frequencies. In this case, ω_1 and ω_2 in the notation of Section 2 are both replaced by the fundamental frequency ω and the mixing frequency $\omega_1+\omega_2$ becomes 2ω Since this ultrathin metasurface has a negligible thickness, there is no issue in *phase-matching* along the direction normal to the metasurface, which is usually the case when using thick nonlinear samples. For oblique illumination with angle of incidence $\theta_{in}=\sin^{-1}(k_z/k_0)$, phase matching on the tangential plane implies that the SHG waves will propagate at the same angle $\theta_{SHG}=\sin^{-1}(\pm 2k_z/2k_0)=\pm\theta_{in}$, where the $\pm$ signs refer to the reflected and transmitted waves, respectively. Here, we consider a normally incident pumping wave with electric field polarized parallel to the nanodipole axis $\mathbf{E}_{inc}=\hat{z}E_0\exp\left[i(k_0x-\omega t)\right]$. After calculating the averaged surface current density (6), we can evaluate the SHG radiated fields on both sides of the surface as

$$\mathbf{E}^{SHG\pm}=-\frac{(2\omega)\mu_0}{(2k_0)}\frac{J_{av}^{NL}}{2}\exp\left[\pm i(2k_0)x\right]\hat{z}. \tag{7}$$

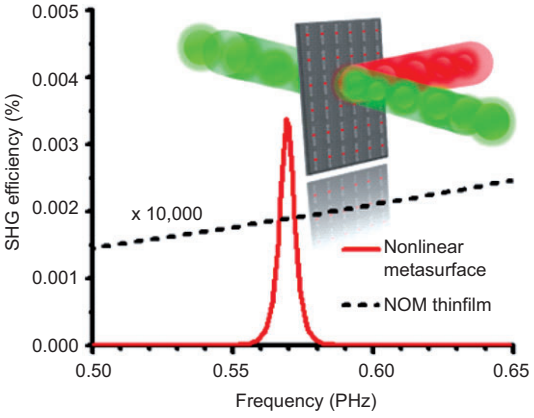

Figure 6 Spectrum of SHG conversion efficiency for a nonlinear metasurface (red solid) compared to a NOM thin film (black dashed), whose magnitude has been magnified 10^4 times for visibility.

The SHG reflection coefficient R^{SHG} is found as the ratio of the amplitude of the nonlinear reflected wave normalized to the incident electric field at the fundamental frequency:

$$R^{SHG}=\frac{-i(2\omega)^2\mu_0}{(2k_0)d_yd_z}\beta(2\omega{:}\omega,\omega)L(2\omega)L(\omega)L(\omega)\left[\frac{2I_0}{c\varepsilon_0}\right]^{1/2}, \tag{8}$$

where I_0 is the power density of the impinging wave at frequency ω. As expected, the SHG transmission coefficient T^{SHG} for forward propagating SHG waves has the same value as R^{SHG} ($T^{SHG}=R^{SHG}$), due to the very small thickness of the metasurface. The conversion efficiency η is given by $\eta=\left|R^{SHG}\right|^2+\left|T^{SHG}\right|^2=2\left|R^{SHG}\right|^2$. We consider a pumping wave with frequency around the nanoantenna resonance frequency $\omega/2\pi=285$ THz and a reasonably high power density $I_0=50$ MW/cm^2. A nanoload with linear permittivity $\varepsilon_L=12.5$ and second-order susceptibility $\chi^{(2)}=250$ pm/V is also considered (i.e., typical values for III–V compounds, such as GaAs and $CdGeAs_2$ [65]). Figure 6 shows the calculated SHG conversion efficiency over the spectrum for this nonlinear metasurface with periods $d_y=250$ nm and $d_z=1.8\ d_y$. A sharp peak of SHG signal is observed with a conversion efficiency $\eta^{SHG}=0.0034\%$. Albeit small, this value is much larger than the SHG conversion efficiency of a NOM uniform thin film with same thickness, which is calculated as $\eta^{SHG}=\tanh^2[\zeta]/\mathrm{sech}^2[0]=1.898\times10^{-7}\%$ [65], where $\zeta=x/l$ is the normalized distance parameter, x is the distance from the crystal interface and $l=\left[2\left(\varepsilon_L(\omega)\right)^2\varepsilon_L(2\omega)\epsilon_0c^3/I_0\right]^{1/2}/(\omega\chi^{(2)})$. This dramatic enhancement ($\sim10^4$ order) is due to the plasmonic nanoantenna resonance at the fundamental frequency. As expected, higher SHG efficiency may be obtained by stacking more of such metasurfaces (although then phase matching should be carefully considered), or by introducing in the design optical nanocavities or nanoresonators to further boost the SHG signal. This nonlinear metasurface may benefit various applications based on SHG effects, paving the way to near-field imaging and spectroscopy, chemical sensing, localized photon sources and active photonic and plasmonic nanodevices. We are currently exploring some of these applications. In addition, this concept can be straightforwardly applied to other frequency mixing or wavelength conversion applications: by loading a $\chi^{(3)}$ NOM, we may be able to obtain enhanced third harmonic generation (THG) or the sum/difference frequency generation, provided that nanoantennas are properly designed to support local field enhancement at each harmonic, which may be realized by suitable nanoantenna designs with dual or multiple frequency bands of operation.

4.2. Phase conjugation and time reversal

One of the most popular applications of metamaterials and metasurfaces is sub-wavelength imaging, beyond the limits of conventional diffractive optics [22, 66–70]. Maslovski and Tretyakov [67] have proposed an interesting alternative approach to 'perfect lensing', based on *phase-conjugation* (or *time reversal* in signal theory), where a pair of ideal phase-conjugating surfaces may electromagnetically resemble a

negative-index slab, without requiring the presence of lossy metamaterial inclusions which are designed to amplify the evanescent spectrum. Phase conjugation, a typical nonlinear process [68, 69], has been experimentally realized at microwaves by employing signal-mixers and nonlinearly loaded RF dipoles. As discussed above, the possibility of exploiting plasmonic effects in nanoantennas may largely enhance these properties at higher frequencies. Indeed, in the realm of optics, Pendry [70] has theoretically shown that this imaging setup may be ideally translated to the visible FWM processes [71, 72], where an ideal *perfect lens* may be achieved using a pair of parallel ultrathin layers, supporting an infinitely large nonlinear response [71, 72]. However, the very weak optical nonlinearities of naturally available NOM thin films may make difficult the practical implementation of this concept, and this ideal setup may require unrealistic pumping levels to achieve sufficient level of nonlinearity for subwavelength focusing.

We note that the plasmonic metasurfaces described in the previous sections, which combine largely enhanced nonlinear response and an ultrathin geometry, may represent the ideal candidate to realize phase-conjugation at optical frequencies based on degenerate FWM. We have suggested and explored this concept in Ref. [63]. Here, we review this application and put it into context within the general formalism introduced in section 2.

In order to achieve a large phase conjugation effect, we load nanoantennas with $\chi^{(3)}$ nonlinearities in order to induce a degenerate four-wave mixing process over an ultrathin surface. In this case, the array density of metasurface was optimized with dimensions $d_y = 100$ nm and $d_z = 2.5\ d_y$. In addition, we tune the nanoantenna design so that the metasurface collectively resonates at the signal frequency $\omega/2\pi = 320$ THz, causing large reflections and very weak transmission of the impinging signal in its linear operation. For large and undepleted pump levels the drastically enhanced and strong fields at the nanogap can produce a conjugate signal with amplitude significantly larger than the signal wave. The large field enhancement at the nanodipole gap ensures drastic enhancement of the third-order nonlinear response at the nanoload. This is supported over an ultrathin profile, which is similar to the ideal mathematical surface suggested by Pendry for the same purpose. This ensures the efficient generation of phase-conjugate signals through FWM process, as well as the equivalence between reflected and transmitted conjugate signals, necessary for subwavelength imaging.

Figure 7A illustrates the operation principle of one phase-conjugating metasurface: the degenerate FWM process is operated by exciting the metasurface with a monochromatic signal wave at frequency ω and two strong, undepleted counterpropagating pump waves at the same frequency (so that $\vec{k}_{p1}+\vec{k}_{p2}=0$). A nonlinear dipole moment with conjugate phase ($\vec{k}_r^{\,pc}=-\vec{k}_s$) is then generated at the nanogap nonlinear load after considering phase-matching [71]. We assume the signal field to be composed of an arbitrary superposition of transverse-electric (TE) impinging wave, linearly polarized with electric field along the nanoantenna axis $\hat{z}$ (Figure 7A): $\mathbf{E}_s = \hat{z}\int_{\infty} E_0(\mathbf{k}_{\|})\exp(i\,\mathbf{k}_{\|}\cdot\mathbf{r}+k_x x)\exp(-i\omega t)\,d\mathbf{k}_{\|}$, with $\mathbf{r}=y\,\hat{\mathbf{y}}+z\,\hat{z}$, $\mathbf{k}_{||}$ being the projection of the wave vector $\mathbf{k}_s$ on the array, and E_0 being an arbitrary amplitude coefficient weights for each component of the impinging signal. This effectively represents an arbitrary source distribution in the transverse plane, to be imaged. After degenerate FWM, each nanoantenna load will support, in addition to its linear dipole moment, a phase-conjugated dipole moment at the mixing frequency $\omega=\omega+\omega-\omega$. Similar to the SHG process considered in the previous section, the total dipole moment at frequency ω for each nanoantenna is then given by

$$\mathbf{p}^{pc}(\omega)=\alpha(\omega)\mathbf{E}_{loc}(\omega)+\gamma(\omega{:}\omega,\omega,-\omega)\mathbf{E}_{loc}(\omega)\mathbf{E}_{loc}(\omega)\mathbf{E}^{*}_{loc}(-\omega) \tag{9}$$

where $\gamma(\omega{:}\omega,\ \omega,\ -\omega)$ is the second hyperpolarizability, accounting for hyper-Rayleigh scattering $\gamma(\omega{:}\omega,\omega,-\omega)=\chi^{(3)}\varepsilon_0\pi a^2 h f_g^4(\omega)$ [8, 11]. After some algebraic manipulation, we may write the phase-conjugate expression as:

$$\mathbf{p}^{pc}(\omega)=\gamma(\omega{:}\,\omega,\omega,-\omega)\Im(\omega)\Im(\omega)\Im(\omega)\Im(-\omega)\,\mathbf{E}_{p1}(\omega)\mathbf{E}_{p2}(\omega)\mathbf{E}^{*}_{s}(-\omega). \tag{10}$$

Similar to (6), the polarization fields supported by the subwavelength periodic array collectively radiate the fundamental diffraction order, or zero-order Floquet mode, sustained by the averaged current density $\mathbf{J}^{pc}_{av}=-i\omega\,\mathbf{p}^{pc}(\omega)\big/d_y d_z$. This averaged current distribution supports phase-conjugate plane waves on either side of the array, as illustrated in Figure 7A. Each phase conjugation plane wave has wave vectors $\mathbf{k}_r^{p.c.}=-\mathbf{k}_{\|}-\mathbf{k}_z$ and $\mathbf{k}_t^{p.c.}=-\mathbf{k}_{\|}+\mathbf{k}_z$ on the two sides of the array, respectively. We may define the reflection coefficient for each phase conjugated wave R^{pc} as the ratio between the amplitude of the backwardly propagating phase-conjugate wave to that of the incident signal wave:

$$R^{pc}=-\frac{i\omega^2\mu_0}{2\sqrt{k_0^2-\mathbf{k}_{\|}^2}\,d_y d_z}\gamma(\omega{:}\omega,\omega,-\omega)L(\omega)L(\omega)L(-\omega)\left(\frac{4I_{p1}I_{p2}}{c^2\varepsilon_0^2}\right), \tag{11}$$

where I_{p1}, I_{p2} are the impinging flux intensity of the pumping waves. For large pump levels, R^{pc} in equation (11) may be much larger than unity, and dominate the linear response of metasurface at frequency ω. Following the theoretical proposal in Ref. [63], we then combine two of such highly-reflective metasurfaces separated by a distance d (see sketch in Figure 7B). In the limit of large $R^{pc}=T^{pc}$, this combination can effectively reproduce the same effect as a negative-refraction planar slab. The total transmission of phase-conjugate waves behind the second metasurface (Figure 7B) may be written as [70]:

$$\mathbf{E}(x)=\hat{z}E_0\frac{\left(R^{pc}\right)^2 e^{i\mathbf{k}_{\|}\cdot\mathbf{r}_{\|}-i\sqrt{k_0^2-\mathbf{k}_{\|}^2}(|x-x'|-2d)-i\omega t}}{1-\left(R^{pc}\right)^2},\ \text{for real}\ \sqrt{k_0^2-\mathbf{k}_{\|}^2} \tag{12}$$

$$\mathbf{E}(x)=\hat{z}E_0\frac{\left(R^{pc}\right)^2 e^{i\mathbf{k}_{\|}\cdot\mathbf{r}_{\|}+i\sqrt{k_0^2-\mathbf{k}_{\|}^2}|x-x'|-i\omega t}}{1-\left(R^{pc}\right)^2 e^{i2\sqrt{k_0^2-\mathbf{k}_{\|}^2}d}},\ \text{for imaginary}\ \sqrt{k_0^2-\mathbf{k}_{\|}^2}, \tag{13}$$

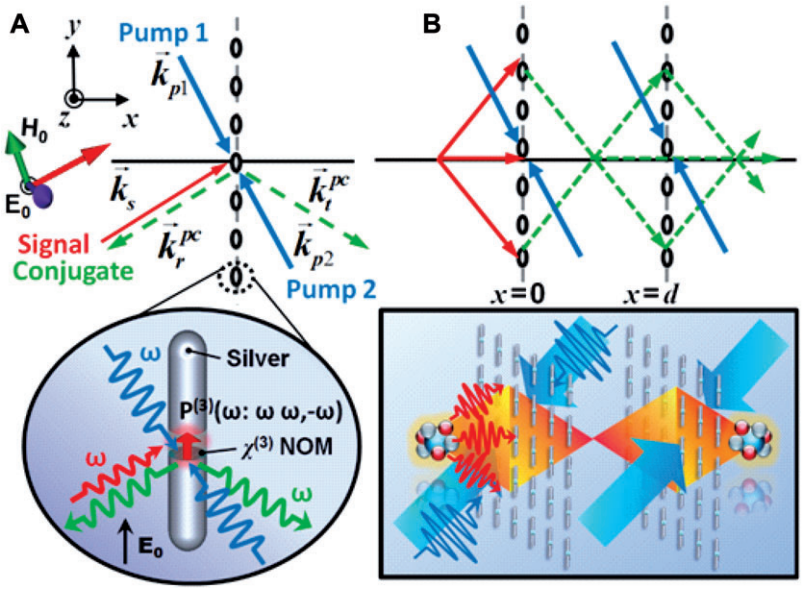

Figure 7 (Color online) Schematic diagram (top view) of: (A) phase-conjugation with a single nanoantenna metasurface through nonlinear four-wave mixing; (B) imaging device formed by two phase-conjugating metasurfaces. Reprinted with permission from [63]. Copyright (2011) American Chemical Society.

which, in the limit $R^{pc}\to\infty\forall\mathbf{k}_{||}$, corresponds to an ideal imaging system in the region $d<x<2d$, for an object placed at $-d<x<0$. We note that for a single metasurface T^{img} is dramatically non-uniform and amplified, which may cause large image distortions for the superposition integral $\mathbf{E}_s$ [63]. However, by considering a pair of phase-conjugating metasurfaces with sufficiently large level of R^{pc}, the transmission on the image plane T^{img} is quite uniform over a wide range of transverse wave vectors (see Ref. [63]). We now consider a practical scenario with two equal-intensity pump waves with power density $I_{p1}=I_{p2}=50$ MW/cm^2 and $\chi^{(3)}=10^{-16}$m^2/V^2 (consistent with realistic values for some polydiacetylenes [73, 74], and realistic silver losses at $\omega/2\pi=320$ THz.

Figure 8A shows the corresponding image plane field distribution at $x=3d/2$, for a sub-wavelength source placed at $x=-d/2$. We show the different cases of: (1) object plane (solid black line), (2) no device between object and image plane (gray dashed line), where diffraction dominates and (3) a pair of metasurfaces (red solid line), which is found to significantly restore the sub-wavelength resolution in the image plane. It is also seen in Figure 8A that the frequency response for different frequencies around the resonance $\omega_0/2\pi=0.320$ PHz, showing a relatively good bandwidth of the subwavelength focusing effect, despite the fact that deterioration is expected due to lower levels of R^{pc} off-resonance. We note that sub-wavelength resolution over a moderate bandwidth of operation is obtained, even after considering realistic levels of absorption in silver. Furthermore, this system allows increasing the distance among metasurfaces and obtains similar sub-wavelength imaging properties, which is much more robust than the equivalent setup obtained with a metamaterial perfect lens [70]. Figure 8B shows the imaging properties of a pair of metasurfaces with distance ranging from $d=0.5\lambda_0$ to $d=3\lambda_0$. Here, a robust subwavelength imaging performance is observed, even for larger distances. We have also considered a larger, but still realistic, pump intensity $I_{p1}=I_{p2}=1$ GW/cm^2 for the case $d=3\lambda_0$ (dash-dot light blue line), verifying that resolution may be enhanced over larger distances by increasing the pumping levels and the corresponding value of R^{pc}.

4.3. Optical bistability effects

In this section, we propose to use plasmonic metasurfaces loaded with $\chi^{(3)}$ NOM, similar to the arrays we considered in the previous sections, to realize enhanced effects of optical bistability (AC Kerr effect) and optical switching [32]. We analyze the scattering and effective homogenized properties of individual and collections of optical nanoantennas loaded with nonlinear $\chi^{(3)}$ Kerr nanoparticles, with relative permittivity $\varepsilon_{load}=\varepsilon_L+\chi^{(3)}\left|E_g\right|^2$, $\varepsilon_L=2.2$, $\chi^{(3)}=4.4\times10^{-20}$ m^2/V^2, typical values for fused silica [65]. We have recently shown how the concepts of antenna loading, tuning and matching may be fully introduced in plasmonic nanoantenna design [16–20], where the nanoparticles' interactions with light can be treated as lumped nanocircuit elements; note that at the infrared/optical frequencies metals [$Re(\varepsilon)<0$] and dielectrics [$Re(\varepsilon)>0$] behave as inductive and capacitive, respectively [26]. Since the nanoantenna properties can be straightforwardly controlled and tuned by the nanoload properties placed at the gap, where the electric field is strongly enhanced, we first investigate the scattering and radiation properties of a single nanoantenna loaded with $\chi^{(3)}$ NOM, and then extend the concept to 2-D arrays. In this case, we consider the same silver nanoantenna with metasurface array density $d_y=100$ nm and $d_z=1.5\,d_y$. Here, we use the semi-analytical method proposed

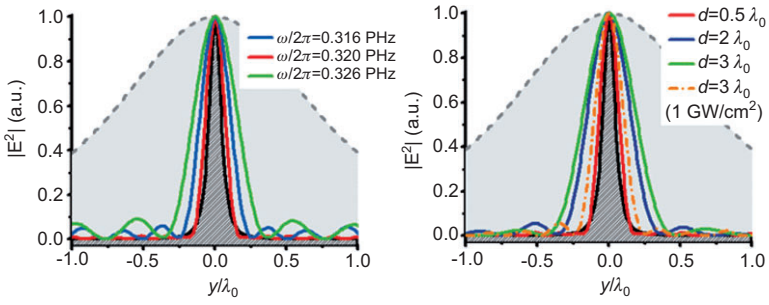

Figure 8 (Color online) Field distribution at the source (black solid), and image plane for the case of: no metasurfaces (gray dash), and double phase-conjugating metasurfaces (colored solid) for different (A) frequencies of operation and (B) separation distances between two metasurfaces. The dash-dot orange line in (B) is for a larger pump intensity of 1 GW/cm^2.

in Ref. [32] to calculate the nonlinear response of these optical nanoantennas, using optical nanocircuit concepts. Figure 9A shows the maximum scattering cross-section σ_{max} vs. wavelength for an individual nanoantenna for light intensity $I=12$ MW/cm^2. It is evident that a bistable loop is obtained in terms of scattering response, associated with the bistability of the load impedance. Farther away from the resonant wavelength, in the long-wavelength regime, the maximum available scattering cross-section smoothly increases with the wavelength of light, following its linear response (red line in Figure 9A). At a certain critical point, however, the increase in enhanced field at the nanogap, associated with the plasmonic resonance, produces a sudden jump to the second stability branch. After this discontinuous transition, if we start decreasing λ, the scattering cross-section will jump back to the initial stability branch, forming a bistable loop associated with the nonlinear response of the nanoload. It is noticed that we can apply the nanocircuit concepts to predict and tailor this bistability using simple loading design formulas for the nanodipoles, as we have discussed in Ref. [32]. It is also shown in our previous work [75, 76] that the hysteresis loops may be tailored with light intensity, and a larger bistable loop may be obtained by increasing the impinging flux intensity. The nonlinear properties of the nanoload also allow envisioning a self-tunable resonant nanoantenna, whose resonance frequency may depend on the impinging light intensity. These hysteresis effects may have appealing applications in realizing all-optical nanomemories and nanoswitches at the nanoscale, since the nanoantenna may have two different stable states for the same applied optical intensity, which depend on the previous history of wavelength or intensity applied to the system. The inset of Figure 9A proposes one possible realization scheme: the nonlinear nanoantenna may be fed by a scanning near-field optical microscope (SNOM) probe, collecting the far-field scattering with photodetectors. This set-up is advantageous over currently available configurations for near-field imaging. The levels of optical intensities that may trigger this behavior are relatively low, due to the large field enhancement at the gap associated with surface plasmon polarization effects of the nanoantenna, squeezing and enhancing the stored optical energy within a small gap height. Figure 9B reports the transmission through a nanoantenna metasurface for impinging intensity $I=470$ MW/cm^2, showing that a similar bistable loop is experienced in terms of the overall metasurface transmissivity. Depending on the metasurface design, a higher level of flux intensity is required to realize an optical bistable loop, due to quenching effects associated with too close coupling between neighboring nanoantennas [32, 64]. It

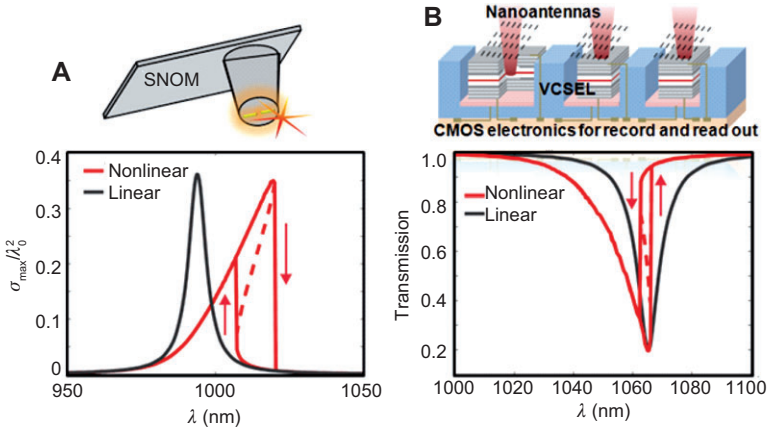

Figure 9 (Color online) (A) Normalized maximum scattering cross-section vs. wavelength for linear (black line) and nonlinear operation (red line) for an individual nanoantenna at a luminous flux of $I=12$ MW/cm^2. (B) Transmission coefficient vs. wavelength for linear (black line) and nonlinear operation (red line) for an array of nanoantennas at a relative high luminous flux of $I=470$ MW/cm^2. The unstable branches of the bistable curves are shown with dashed lines.

is seen that when the operation wavelength is getting close to the resonance of nanoantenna arrays in the linear regime (at a weak incident flux; red line), an analogous bistable behavior is triggered for the overall metasurface response, producing an intensity-dependent, self-tunable reflection and transmission properties. Such hysteresis effect may be interesting to realize compact and chip-scale, all-optical nanomemory or nanoswitch nanodevices [shown in the inset of Figure 9B], as well as intensity-tunable infrared/optical impedance surfaces. It is found that a relatively low incident power may support bistability and switching effects, of great interest in a variety of optical nanodevices [32]. Based on similar concepts, an actively-tunable bistable Yagi-Uda nanoantenna array has been recently proposed [77]. Unlike its narrowband unloaded counterparts, this nonlinear Yagi-Uda nanoantenna array exhibits a broadband unidirectional emission and a bistable response in a preferential far-field direction.

Strong bistability and self-tunability effects associated with the nonlinear response of nanoantennas may drastically enhance the available degrees of freedom of linear optical nanoantennas and metasurfaces, enabling fascinating applications for novel optical nanodevices and self-tunable surfaces. We also envision the employment of stacked metasurfaces for the realization of metamaterials with enhanced nonlinear properties, as well as tunable and switchable effective material profiles, which could be varied from positive to near-zero or negative values [75, 76].

5. Conclusions

In this work, we have reviewed the use and a few applications of nanoantennas to boost nonlinear optical effects and operations. We have first discussed the large body of recent works utilizing the surface nonlinear susceptibility of metallic nanoparticles. We have then discussed how, by loading suitably tailored nanoantennas with nonlinear particles, we may be able to fully characterize, enhance and control their optical nonlinear response similar to radio-frequency nonlinearly loaded antennas. We have shown that planar arrays of these elements may be described as nonlinear metasurfaces, providing interesting potentials for boosting optical nonlinearities, with application in nonlinear wave mixing, phase conjugation and optical bistability. The proposed ultrathin nonlinear metasurfaces may provide practical venues to realize nanoscale frequency converters (nanomixers) and super-resolving imaging devices, which may allow relatively long-distance subwavelength imaging. All-optical nanomemories and nanoswitches may also be operated with relatively low flux intensity values. Their figures of merit are far superior to currently available nonlinear optical devices and the demonstrated concepts may be applied to coherent and frequency-tunable local photon sources, near-field imaging and spectroscopy, chemical sensing, subwavelength imaging system, logical unit cells for optical computing, on-chip communication and active plasmonics. We finally note that the aforementioned effects may be further amplified when considering the strong real part of the inherent $\chi^{(3)}$ nonlinearity in metallic nanoparticles [78].

Acknowledgements

This work has been partially supported by the ARO STTR project "Dynamically Tunable Metamaterials", AFOSR with the YIP award No. FA9550-11-1-0009 and the ONR MURI grant No. N00014-10-1-0942.

References

[1] Hutter E, Fendler JH. Exploitation of localized surface plasmon resonance. Adv Mater 2004;16:1685–706.
[2] Sweatlock LA, Maier SA, Atwarter HA, Penninkhof JJ, Polman A. Highly confined electromagnetic fields in arrays of strongly coupled Ag nanoparticles. Phys Rev B 2005;71:235408.
[3] Alù A, Engheta N. Theory of linear chains of metamaterial/plasmonic particles as subdiffraction optical nanotransmission lines. Phys Rev B 2006;74:205436.
[4] Jain PK, Huang X, El-Sayed H, El-Sayed MA. Noble metals on the nanoscale: optical and photothermal properties and some applications in imaging, sensing, biology, and medicine. Acc Chem Res 2008;41:1578–86.
[5] Ebbesen, TW, Lezec HJ, Ghaemi HF, Thio T, Wolff PA. Extraordinary optical transmission through sub-wavelength hole arrays. Nature (Lond) 1998;391:667–9.
[6] Scalora M, D'Aguanno G, Mattiucci N, Bloemer MJ, de Ceglia D, Centini M, Mandatori A, Sibilia C, Akozbek N, Cappeddu MG, Fowler M, Haus JW. Negative refraction and sub-wavelength focusing in the visible range using transparent metallodielectric stacks. Opt Express 2007;15:508–23.
[7] Shalaev VM. Optical negative-index metamaterials. Nat Photon 2007;1:41–8.
[8] Ricard D, Roussignol O, Flytzanis C. Surface-mediated enhancement of optical phase conjugation in metal colloids. Opt Lett 1985;10:511–3.
[9] Klar T, Perner M, Grosse S, Plessen G, Spirkl W, Feldmann J. Surface-plasmon resonances in single metallic nanoparticles. Phys Rev Lett 1998;80:4249–52.
[10] Kelly KL, Coronado E, Zhao LL, Schatz GC. The optical properties of metal nanoparticles: the influence of size, shape, and dielectric environment. J Phys Chem B 2003;107:668–77.
[11] Pu Y, Grange R, Hsieh CL, Psaltis D. Nonlinear optical properties of core-shell nanocavities for enhanced second-harmonic generation. Phys Rev Lett 2010;104:207402.
[12] Danckwerts M, Novotny L. Optical frequency mixing at coupled gold nanoparticles. Phys Rev Lett 2007;98:026104.
[13] Palomba S, Novotny L. Near-field imaging with a localized nonlinear light source. Nano Lett 2009;11:3801–4.
[14] Navarro-Cia M, Maier SA. Broad-band near-infrared plasmonic nanoantennas for higher harmonic generation. ACS Nano 2012;6:3537–44.
[15] Maier SA. Plasmonic field enhancement and SERS in the effective mode volume picture. Opt Express 2006;14:1957–64.
[16] Muhlschlegel P, Eisler HJ, Martin OJF, Hecht B, Pohl DW. Resonant optical antennas. Science 2005;308:1607–9.
[17] Novotny L, Hulst NV. Antennas for light. Nat Photonics 2011;5:83–90.
[18] Biagioni P, Huang JS, Hecht B. Nanoantennas for visible and infrared radiation. Rep Prog Phys 2012;75:024402.
[19] Alù A, Engheta N. Tuning the scattering response of optical nanoantennas with nanocircuit loads. Nat Photonics 2008;2:307–10.
[20] Alù A, Engheta N. Input impedance, nanocircuit loading, and radiation tuning of optical nanoantennas. Phys Rev Lett 2008;101:043901.

[21] Sorger VJ, Oulton RF, Yao J, Bartal G, Zhang X. Submicrometer in-plane integrated surface plasmon cavities. Nano Lett 2009;9:3489–93.
[22] Fang N, Lee H, Sun C, Zhang X. Sub-diffraction-limited optical imaging with a silver superlens. Science 2005;308:534–7.
[23] Shvets G, Urzhumov YA. Engineering the electromagnetic properties of periodic nanostructures using electrostatic resonances. Phys Rev Lett 2004;93:243902.
[24] Alù A, Engheta N. Achieving transparency with plasmonic and metamaterial coatings. Phys Rev E 2005;72:016623.
[25] Cai W, Chettiar UK, Kildshev AV, Shalaev VM. Optical cloaking with metamaterials. Nat Photon 2007;1:224–7.
[26] Engheta N, Salandrino A, Alù A. Circuit elements at optical frequencies: nanoinductors, nanocapacitors, and nanoresistors. Phys Rev Lett 2005;95:095504.
[27] Huang W, Quian W, Jain PK, El-Sayed MA. The effect of plasmon field on the coherent lattice phonon oscillation in electron-beam fabricated gold nanoparticle pairs. Nano Lett 2007;7:3227–34.
[28] Popov AK, Myslivets SA, Shalaev VM. Coherent nonlinear-optical energy transfer and backward-wave optical parametric generation in negative-index metamaterials. Physica B 2010;405:2999–3002.
[29] Lippitz M, van Dijk MA, Orrit M. Third-harmonic generation from single gold nanoparticles. Nano Lett 2005;5:799–802.
[30] Hanke T, Krauss G, Trautlein D, Wild B, Bratschitsch R, Leitenstorfer A. Efficient nonlinear light emission of single gold optical antennas driven by few-cycle near-infrared pulses. Phys Rev Lett 2009;103:257404.
[31] Canfield BK, Hush H, Laukkanen J, Bai B, Kuittinen M, Turunen J, Kauranen M. Local field asymmetry drives second-harmonic generation in non-centrosymmetric nanodimers. Nano Lett 2007;7:1251–5.
[32] Klein MW, Enkrich G, Wegener M, Linden S. Second-harmonic generation from magnetic metamaterials. Science 2006;313:502–4.
[33] Chen PY, Alù A. Optical nanoantenna arrays loaded with nonlinear materials. Phys Rev B 2010;82:235405.
[34] Novotny L. Effective wavelength scaling for optical antennas. Phys Rev Lett 2007;98:266802.
[35] Huang JS, Feichtner T, Biagioni P, Hecht B. Impedance matching and emission properties of nanoantennas in an optical nanocircuit. Nano Lett 2009;9:1897–902.
[36] Zhao Y, Engheta N, Alù A. Effects of shape and loading of optical nanoantennas on their sensitivity and radiation properties. JOSA B 2011;28:1266–74.
[37] Giannini V, Fernández-Domínguez AI, Heck SC, Maier SA. Plasmonic nanoantennas: fundamentals and their use in controlling the radiative properties of nanoemitters. Chem Rev. 2011;111:3888–912.
[38] Knight MW, Sobhani H, Nordlander P, Halas NJ. Photodetection with active optical antennas. Science 2011;332:702–4.
[39] Kotter DK, Novack SD, Slafer WD, Pinhero PJ. Theory and Manufacturing processes of solar nanoantenna electromagnetic collectors. J Sol Energy Eng 2010;132:011014.
[40] Harutyunyan H, Volpe G, Quidant R, Novotny L. Enhancing the Nonlinear optical response using multifrequency gold-nanowire antennas. Phys Rev Lett 2012;108:217403.
[41] Malyuskin O, Fusco V, Schuchinsky AG. Microwave phase conjugation using nonlinearly loaded wire arrays. IEEE Trans Antenna Propagat 2006;54:192–203.
[42] Shadrivov IV, Morrison SK, Kivshar YS. Tunable split-ring resonators for nonlinear negative-index metamaterials. Opt Express 2006;14:9344–9.
[43] Powell DA, Shadrivov IV, Kivshar YS. Self-tuning mechanisms of nonlinear split-ring resonators. Appl Phys Lett 2007;91:144107.
[44] Slobozhanyuk AP, Kapitanova PV, Shadrivov IV, Belov PA, Kivshar YS. Metamaterials with tunable nonlinearity. JETP Lett 2012;95:613–7.
[45] Lapine M, Shadrivov I, Kivshar Y. Wide-band negative permeability of nonlinear metamaterials. Sci Rep 2012;2:1–4.
[46] Boyd RW, Gehr RJ, Fischer GL, Sipe JE. Nonlinear optical properties of nanocomposite materials. Pure Appl Opt 1996;5:505–12.
[47] Smith DD, Fischer G, Boyd RW, Gregory DA. Cancellation of photoinduced absorption in metal nanoparticle composites through a counterintuitive consequence of local field effects. J Opt Soc Am B 1997;14:1625–31.
[48] Bharadwaj P, Deutsch B, Novotny L. Optical antennas. Adv Opt Photon 2009;1:438–83.
[49] Scholl JA, Koh AL, Dionne JA. Quantum plasmon resonances of individual metallic nanoparticles. Nature 2012;483:421–8.
[50] Ciracì C, Hill RT, Mock JJ, Urzhumov Y, Fernández-Domínguez AI, Maier SA, Pendry JB, Chilkoti A, Smith DR. Probing the ultimate limits of plasmonic enhancement. Science 2012;337:1072–4.
[51] Renger J, Quidant R, Novotny L. Enhanced nonlinear response from metal surfaces. Opt Express 2011;19:1777–85.
[52] Palomba S, Danckwerts M, Novotny L. Nonlinear plasmonics with gold nanoparticle antennas. J Opt A: Pure Appl Opt 2009;11:114030.
[53] Esteban R, Borisov AG, Nordlander P, Aizpurua J. Bridging quantum and classical plasmonics with a quantum-corrected model. Nature Commun 2012;3:825.
[54] Liu N, Langguth L, Weiss T, Kastel J, Fleischhauer M, Pfau T, Giessen H. Plasmonic analogue of electromagnetically induced transparency at the Drude damping limit. Nat Mater 2009;8:758–62.
[55] Zhang S, Genov DA, Want Y, Liu M, Zhang X. Plasmon-induced transparency in metamaterials. Phys Rev Lett 2008;101:047401.
[56] Mukherjee S, Sobhani H, Lassiter JB, Nordlander P, Halas NJ. Fano shells: nanoparticles with built-in Fano resonances. Nano Lett 2010;10:2694–701.
[57] Argyropoulos C, Chen PY, Monticone F, D'Aguanno G, Alù A. Nonlinear plasmonic cloaks to realize giant all-optical scattering switching. Phys Rev Lett 2012;108:263905.
[58] Chang DE, Sorensen AS, Demler EA, Lukin MD. A single photon transistor using nanoscale surface plasmons. Nat Phys 2007;3:807–12.
[59] Johnson PB, Christy RW. Optical constants of the noble metals. Phys Rev B 1972;6:4370–9.
[60] CST Microwave Studio v. 2012: http://www.cst.com/. Accessed on 1 November 2012.
[61] Fischer H, Martin OJF. Engineering the optical response of plasmonic nanoantennas. Opt Express 2008;16:9144–54.
[62] Alù A, Engheta N. Optical wave interaction with two-dimensional array of plasmonic nanoparticles. In: Maradudin AA, editor. Structured surfaces as optical metamaterials. Chapter 3. Cambridge: Cambridge University Press; 2011, pp. 58–93.
[63] Chen PY, Alù A. Subwavelength imaging using phase-conjugating nonlinear nanoantenna arrays. Nano Lett 2011;11:5514–8.
[64] Belov PA, Simovski CR. Homogenization of electromagnetic crystals formed by uniaxial resonant scatterers. Phys Rev E 2005;72:026615.
[65] Boyd RW. Nonlinear optics. 3rd edition. Boston, MA: Academic Press; 2008.

[66] Pendry J. Negative refraction makes a perfect lens. Phys Rev Lett 2000;85:3966–9.
[67] Maslovski S, Tretyakov S. Phase conjugation and perfect lensing. J Appl Phys 2003;94:4241–3.
[68] Malyuskin O, Fusco V, Schuchinsky A. Phase conjugating wire FSS lens. IEEE Trans Antenna Propagat 2006;54:1399–404.
[69] Katko AR, Gu S, Barrett J, Popa B, Shvets G, Cummer SA. Phase conjugation and negative refraction using nonlinear active metamaterials. Phys Rev Lett 2010;105:123905.
[70] Pendry JB. Time reversal and negative refraction. Science 2008;322:71–3.
[71] Yariv A. Phase conjugate optics and real-time holography. IEEE J Quan Electron 1978;14:650–60.
[72] Palomba S, Zhang S, Park Y, Bartal G, Yin X, Zhang X. Optical negative refraction by four-wave mixing in thin metallic nanostructures. Nat Mater 2011;11:34–8.
[73] Sirtori C, Capasso F, Sivco DL, Cho AY. Giant, triply resonant, third-order nonlinear susceptibility chi 3 omega (3) in coupled quantum wells. Phys Rev Lett 1992;68:1010–3.
[74] Hamazaki J, Matsui S, Kunugita H, Ema K, Kanazawa H, Tachibana T, Kikuchi A, Kishino K. Ultrafast intersubband relaxation and nonlinear susceptibility at 1.55 μm in GaN/AlN multiple-quantum wells. Appl Phys Lett 2004;84:1102–4.
[75] Chen PY, Farhat M, Alù A. Bistable and self-tunable negative-index metamaterials at optical frequencies. Phys Rev Lett 2011;106:105503.
[76] Argyropoulos C, Chen PY, D'Aguanno G, Engheta N, Alù A. Boosting optical nonlinearities in epsilon-near-zero plasmonic channels. Phys Rev B 2012;85:045129.
[77] Maksymov IS, Miroshnichenko AE, Kivshar YS. Actively tunable bistable optical Yagi-Uda nanoantenna. Opt Express 2012;20:163243.
[78] Drachev VP, Buin AK, Nakotte H, Shalaev VM. Size Dependent $\chi^{(3)}$ for conduction electrons in Ag nanoparticles. Nano Lett 2004;4:1535.

Received April 9, 2012; accepted October 29, 2012